

Composites of resonant dielectric rods: A test of their behavior as metamaterial refractive elements

F.J. Valdivia-Valero¹ and M. Nieto-Vesperinas¹¹

¹¹*Instituto de Ciencia de Materiales de Madrid, C.S.I.C., Campus de Cantoblanco
28049 Madrid, Spain*

We report numerical experiments of optical wave propagation in composites of high refractive index dielectric rods at frequencies where their first electric and magnetic Mie resonances are excited. The arrays of these particles have been extensively studied and proposed as non-absorbing and isotropic metamaterials. We show that negative refraction, observed in ordered particle arrays, is due to diffraction and that an effective medium theory yields constitutive parameters that do not reproduce the observations in these composites, whose transmission also depends on the sample shape. This is further confirmed by disordering the arrays, a case in which large transmission losses appear due to extinction by resonant scattering from the particles. Therefore, these composites although little absorbing have large extinction due to scattering.

INTRODUCTION

Progress in metamaterial design, from microwaves to THz and optical frequencies [1–5], based on the magnetic response of arrays of wires and split ring resonators (SRR) and their modifications to shorter electromagnetic waves, shows as essential limitations the existence of anisotropy and large absorption losses [6]. More recently, alternative structures based on Mie scattering by dielectric spheres [6–11] of relative large refractive index were extensively studied and proposed as models of lossless composites at microwaves; these were also extended to semiconductor cylinders and spheres, which were proven to possess similar resonant characteristics in the infrared and visible regions [12, 13]. Although initially these latter structures relied on only the electric dipole or on multipole modes, later the possibility of exciting the first Mie magnetic dipole resonance was realized; which makes these particles equivalent from a fundamental point of view to the microwave wire and SRR elements as far as their electric and magnetic responses are concerned. Moreover, these cylinders and spheres provide isotropy 2D and 3D in addition to their resonance being subwavelength, both for the electric and magnetic excited dipoles. The purpose of this paper is to investigate the transmittance properties of media composed of these dielectric particles and in particular, whether they behave as uniform media at frequencies where their electric and magnetic dipoles are excited. Therefore this work is a test and assessment of whether the excitation of electric and magnetic resonances of high index Mie spheres and cylinders constitutes an alternative with low losses and high refractive transmittivity, to previously developed metamaterial models.

In this connection, we emphasize that in spite of the exhaustive studies on the possibilities of these resonant particles as metamaterial building blocks in [8–13] and references therein, no such a test has been carried out.

Although a unified view of the effective refractive index of metamaterials made of ordered arrays of such particles, as well as of photonic crystals (PC) producing negative refraction [14] was established [15], the characterization of these composites as effective homogeneous media to the propagating wave has generally employed the method of the scattering (S) parameter by inversion of the complex transmittances and reflectances [1]. Then, it remained the question of whether the effective constitutive parameters ϵ_{eff} and μ_{eff} derived from effective medium homogenization procedures commonly employed [8, 9, 11, 13], were the same as those obtained by those methods that took into account the wave interaction with the microstructure of the composite unit cell. The answer, recently given [16], is negative. *The linear dimension of such unit cells, which is typically between $\lambda/10$ and $\lambda/6$, is a much larger number than those of atom or molecule arrangements in transparent dielectrics acting to the pass of light.* In fact, the maximum lattice constant versus wavelength for a metamaterial to behave as an uniform effective medium in negative refraction experiments, was established in [17]. Therefore, one may ask whether reducing absorption of the composite, like with these Mie resonances of dielectric spheres and cylinders, is sufficient to achieving an application as a metamaterial which may be considered as a refractive element.

To this end, we shall see in this paper that, although contrary to metal elements like those of earlier left - handed material (LHM) designs, these dielectric cylinders and spheres grouped as "meta - atoms" of composites do not present absorption, their scattering cross section is quite large. Therefore, *we will demonstrate that this time the losses of light transmission come from their large extinction cross section due to scattering, which moreover, when random arrangements of these particles are also addressed, yields a rather short transport mean free path, even if the medium is homogenized, and hence the transmittivity of a propagating beam through these media is low.*

As a 2-D equivalent to spheres, both ceramic [11] and of Silicon [12], rod array composites were suggested to exhibit metamaterial left-handed behaviour in the microwave and in the visible to mid-infrared (IR) ranges, respectively, due to the excitation of the cylinder magnetic Mie resonance. However, further studies pointed out [18] the necessity of *more research to sort out whether the backward wave behavior inside a periodic array of such Si cylinders is due to the band structure in the diffraction regime [19] or to a pure left-handed effect in the long wavelength range*, even though experiments of microwaves in prisms of large permittivity ceramic rod arrays, either ordered or random, suggested a left-handed behavior [11].

The typical filling fraction f of the studied dielectric cylinder arrays [11–13] is moderate $f \approx 0.30$, but the wavelength in vacuum to rod radius ratio: λ/r was 61 in e. g. the experiment of [11] ($\lambda = 41.64mm$), the lattice constant a to λ ratio being 0.07, which is well below the aforementioned ratio $a/\lambda = 0.1$; whereas $\lambda/r = 9.8$ and $a/\lambda = 0.45$ in the model of the ordered Si cylinders of [12] ($\lambda = 1.55\mu m$). On the other hand, the equivalent homogeneous media obtained from Snell law had an index of negative refraction $n \simeq -0.6$ for the PC slab of [12] and $n \simeq -1.08$ for the PC prism of [11], ($\lambda_n \simeq 2.58\mu m$ for the case of [12], whereas $\lambda_n \simeq 38.5mm$ for [11], $\lambda_n = \lambda/n$). None of these values is maintained when one changes the sample geometry, as we shall prove in this paper.

In the homogenization procedure employed in the ceramic composite of [11], the effective parameters obtained in the band of left-handed behaviour have negative values both for the real part of the magnetic permeability, μ_{eff}^R ,

as for that of the dielectric permittivity, ϵ_{eff}^R , with $\mu_{eff}^R \ll \epsilon_{eff}^R$. However, near the resonance wavelength, the imaginary parts ϵ_{eff}^I and μ_{eff}^I of both constitutive parameters are non - negligible compared to those real parts; *this conveys high extinction by the composite material, which is not due to absorption losses as in previous models of LHM composed of metallic elements, but produced by scattering from the high index particles of these metamaterials.* The same happens in the near IR for the composite material of Si cylinders [12] and [13]. This will be further studied in this work.

In this paper we carry out 2 - D numerical experiments with the finite element method (FEM) of propagation, of mid - IR waves, through a composite medium made of dielectric rods either in periodic or random positions. Nonetheless, for the sake of comprehensiveness, we shall also address the related problem of microwave propagation at larger scales. From the above discussion, our aim is to assess for the first time to what extent these structures may constitute a metamaterial model that overcomes the losses [20, 21] of previous composites. This conveys to discuss the validity of establishing effective constitutive parameters. The results should closely predict laboratory experimental observations because the calculations involved are exact. Since in this model the size of the samples are not huge compared to the wavelength [16, 17], in order to assess whether the propagation depends or not on this size and on the shape of the sample, we employ two of such bodies for observing transmission: a rectangular block, or thick slab, and a prism, (i. e. in the 2-D calculations the latter being a triangle), composed of either a periodic or a disordered array of rods in air. Like in previous studies on these composites, the incident wave is assumed to be linearly polarized with electric vector \mathbf{E} along the cylinder axes.

SETS OF ORDERED AND RANDOM RODS AS METAMATERIALS

Numerical procedure

Maxwell equations are solved by using a finite element method (FE) (FEMLAB of COMSOL, <http://www.comsol.com>). The calculation domain is meshed with element growth rate: 1.55, meshing curvature factor: 0.65, approximately. The geometrical resolution parameters consist of 25 points per boundary segment to take into account curved geometries in order to adapt the finite elements to the geometry and optimize the convergence of the solution. The final mesh contains about 10^4 elements. To solve Helmholtz equation, the UMFPACK direct is employed. The boundary conditions of the simulation space are established both to keep the calculations from undesired window reflections and to avoid possible geometrical discontinuities. We then ensure that no inconsistencies due to properties discontinuities of the objects under study appear, and possible systematic errors are avoided.

In the 2 - D configuration, light depolarization is prevented by launching linearly polarized light with propagation vector in the XY - plane of the cylinder cross sections. Beam profiles are either, rectangular (plane waves): $\mathbf{E}_0 \exp(i(\mathbf{k}_i \cdot \mathbf{r}_i - \omega t))$, their widths being that of the simulation window, or Gaussian: $\mathbf{E}_0 \exp(-|\mathbf{R} - \mathbf{R}_0|^2/2\sigma^2) \exp(i(\mathbf{k}_i \cdot \mathbf{r} - \omega t))$, $\mathbf{r} = (\mathbf{R}, z)$. $\mathbf{R} = (x, y)$ and $\mathbf{R}_0 = (x_0, y_0)$ are the transversal components of \mathbf{r} and \mathbf{r}_0 , respectively, σ is the standard deviation or beam waist, and \mathbf{k}_i is the incident wave wavevector with $|\mathbf{k}_i| = 2\pi/\lambda$. For the wavelength λ , we shall address values either in the microwave or IR regions. The direction of propagation \mathbf{k}_i of such beams is thus normally incident to the OZ - axis of the infinite cylinders. The incident wave amplitude is normalized to $|\mathbf{E}_0| = 1V/m$ (SI), which corresponds to a magnitude of the time average energy flow $|\langle \mathbf{S} \rangle| \approx 190W/m^2$. The criterium to choose the beam profile has been based on the major response of the composite characteristics to analyze: directionality of propagation in the media resulting from an homogenization method, and extinction processes when the inner structure of the rod distribution is considered. In the first case, we employ rectangular incident beams; otherwise, we use Gaussian beams.

The results are thus expressed in terms of either the electric vector $\mathbf{E}(\mathbf{R})$ which points along the cylinder OZ - axis, the squared root of its time - averaged energy $|\mathbf{E}(\mathbf{R})|$, the magnetic vector $\mathbf{H}(\mathbf{R}) = (H_x, H_y)$ or the time average energy flow $\langle \mathbf{S}(\mathbf{R}) \rangle$. These latter two vectors of course being both transversal, namely, in the XY - plane of the images to show next.

Finally, to classify the whispering gallery modes (WGM) associated to the Mie resonances of the cylinders we will use the subscripts (i, j) , i and j standing for their angular i - th and radial j - th orders, respectively.

Electric and magnetic dipolar response of a dielectric cylinder in the microwave and mid - IR regimes

We first address the response of one single ceramic cylinder of $Ba_{0.5}Sr_{0.5}TiO_3$ (BST) to microwaves. Figures 1(a) - (c) show the electric, magnetic and time - averaged Poynting vector distributions for linear polarized illumination

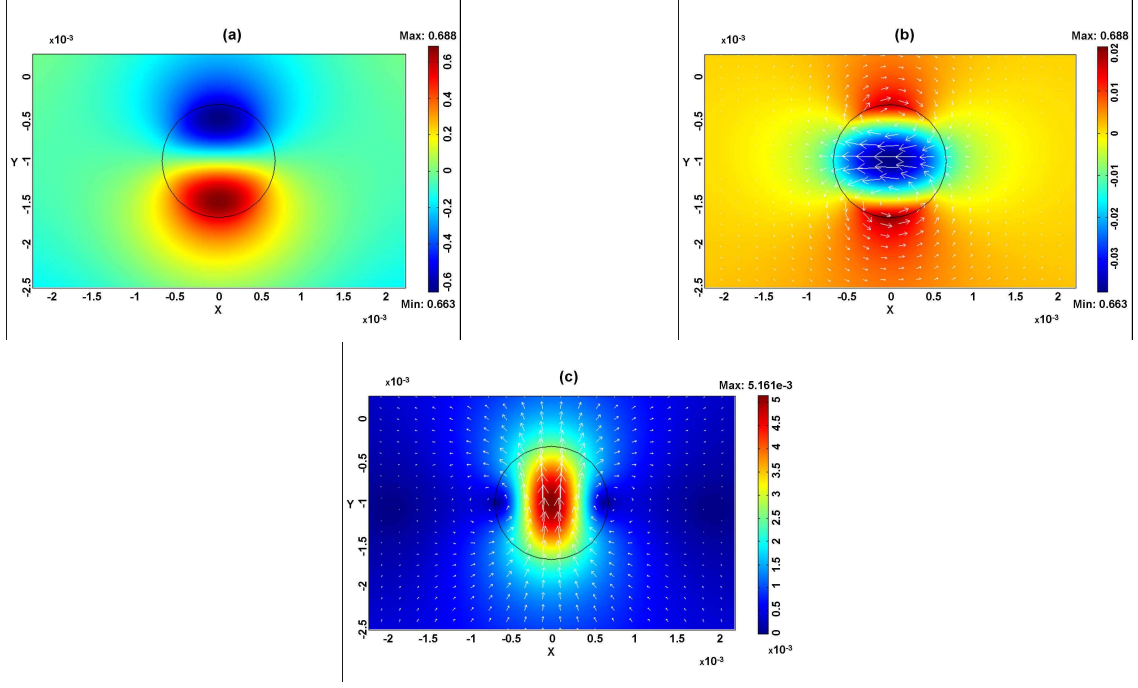


FIG. 1. (a) Electric field $E_z(\mathbf{R})$ in a cylinder of BST ceramic with a dielectric permittivity $\epsilon = 600$ and radius $r = 0.68\text{mm}$. (b) Magnetic field $\mathbf{H}(\mathbf{R})$ (arrows) and its X - component (colors). (c) Averaged energy flow $\langle \mathbf{S}(\mathbf{R}) \rangle$ (arrows) and its norm (colors). In these figures, an s - polarized Gaussian beam of amplitude $A = 1\text{V/m}$ and standard deviation $\sigma = 12\text{mm}$ at $\lambda = 41.638\text{mm}$ is launched upwards (i. e. with \mathbf{R}_i along the OY - axis), from below the cylinder, exciting its $WGM : TM_{1,1}$.

with the electric vector along the cylinder axis. Figure 1(a) exhibits $E_z(\mathbf{R})$, indicating two electric currents flowing along the cylinder OZ - axis, one upwards and one downwards, respectively, and centered near opposite sides of the rod periphery, which corresponds to the \mathbf{E} - spatial distribution of the dipolar $WGM : TM_{1,1}$. Figure 1(b) shows the magnetic vector lines in the XY - plane, characterized by arrows circulating around these electric currents, according to Ampere's law and behaves as that of a magnetic dipole. The time - averaged energy flow, characterized by the mean Poynting vector, is shown in Fig. 1(c) exhibiting an interesting circulation around the equatorial extremes of the cylinder section.

On the other hand, Figs. 2(a) - 2(c) show the response of one single Si cylinder to infrared light. The characteristics quoted above for the BST ceramic cylinder are again reproduced for this Si rod, as expected from the analysis of their similar electric and magnetic resonances [12].

Transmission characteristics of a slab with ordered rod distributions in the microwave regime

We now consider a thick slab made of a periodic array of the BST rods in air whose response was studied in Figs. 1(a) - (c), (see Figs. 3(a) and 3(b)). An s - polarized light beam is launched on this system at angle $\theta = 20^\circ$. The map of transmitted $E_z(\mathbf{R})$ field is shown in Fig. 3(a). A transmission angle $\theta \approx 0^\circ$ is observed within the sample. A resonant field distribution appears within the rods, being somewhat similar to that of Fig. 1(a), taking into account the frequency shifts due to the presence of neighbor rods. On the other hand, Fig. 3(b) shows both the time - averaged electric energy $|E_z(\mathbf{R})|$ and energy flow $\langle \mathbf{S}(\mathbf{R}) \rangle$ in a detail of the block of rods. The latter showing the Bragg directions of propagation inside the crystal. Nevertheless, in the experiment of [11] (cf. Figs. 3 of Ref. [11]) on a prism of an identical array, a refraction angle of about 20° was obtained instead, which would correspond to $n_{eff} \simeq -1.08$. A 75% of transmitted energy is lost in the rod slab of Figs. 3(a) and 3(b).

However, homogenization from an effective medium theory employed like in [11, 13, 22, 23] leads us to estimate for this composite the effective homogeneous medium constitutive parameters $\epsilon_{eff}^R = -36$, $\epsilon_{eff}^I = 14.7$; $\mu_{eff}^R = -0.9$, $\mu_{eff}^I = 0.11$ (see Fig. 4). Such a uniform medium produces an angle of refraction which is very small, similar to that of Fig. 3(a) but does not reproduce the inner structure of the wavefield. This is shown in Figs. 3(c) and 3(d) which display $E_z(\mathbf{R})$ and a detail of $|E_z(\mathbf{R})|$ and $\langle \mathbf{S}(\mathbf{R}) \rangle$ for such an effective medium.

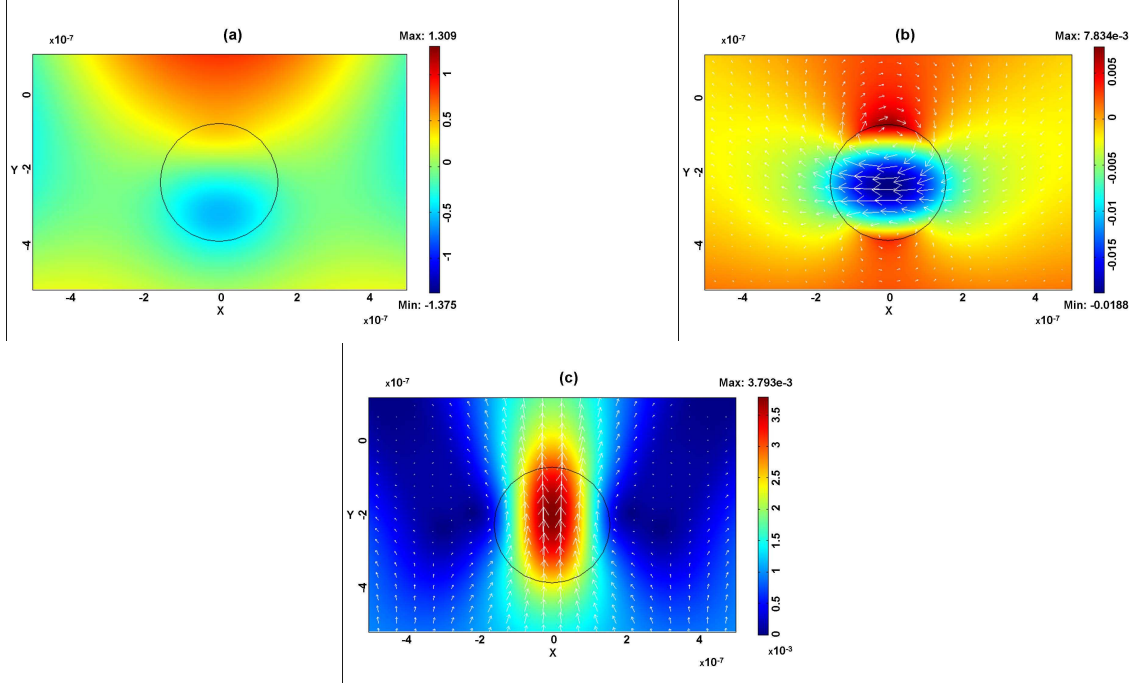


FIG. 2. (a) Electric field $E_z(\mathbf{R})$ in a cylinder of Si with a dielectric permittivity $\epsilon = 12$ and radius $r = 158\text{nm}$. (b) Magnetic field $\mathbf{H}(\mathbf{R})$ (arrows) and its X - component (colors). (c) Averaged energy flow $\langle \mathbf{S}(\mathbf{R}) \rangle$ (arrows) and its norm (colors). An s - polarized Gaussian beam of amplitude $A = 1\text{V/m}$ and standard deviation $\sigma = 2792\text{nm}$ at $\lambda = 1.55\mu\text{m}$ is launched upwards (i. e. with \mathbf{R}_i along the OY direction), from below the cylinder, exciting its $WGM : TM_{1,1}$.

Now a 95% of losses appears in the transmitted energy emerging from the homogeneous medium of Figs. 3(c) and 3(d). These results manifest the very different observed refraction depending on the sample on use: whether it is the composite or we deal with its EMT homogenization. In fact, although not shown here, we remark that we have reproduced the numerical results of [11] for such an array if the sample is a prism which, as said above, yields a refraction completely different to that of Figs. 3(a) and 3(b).

Hence, we infer the questionable matching of an EMT with the observations in such a regular array of rods. This is not surprising in the light of the results of [16] and [17], since the sample in these cases is not much larger than the inner structure, at difference with light transmission experiments in usual light refractive elements of nanoscopic molecular inner structure sizes.

Microwave transmission in a slab with a random distribution of cylinders

Different realizations, obtained by randomizing the array of Figs. 3(a) and 3(b) are now addressed. We next study a disordered distribution of BST rods as those employed in Section ???. Now, there is 85% of transmission losses through the slab of these disordered rods due to extinction produced by scattering. Figs. 5(a) and 5(b) show the field $E_z(\mathbf{R})$ and a detail of both $|E(\mathbf{R})|$ and $\langle \mathbf{S}(\mathbf{R}) \rangle$, respectively. A large amount of scattered light is lost both above and below the slab upper and lower low reflection boundaries. Again some few rods exhibit the excitation of Mie resonances on illumination as in Fig. 1(a). Figures 5(a) and 5(b) yield no clue of a forward transmission direction into the air at the exit of the sample. This result is obtained with both a beam and a plane wave. Although not shown here, we should state that we observed that averaging the field $E_z(\mathbf{R})$ over many realizations of the random distribution of rods does not yield a forwardly transmitted beam, characterized by $\langle E_z(\mathbf{R}) \rangle$ [24–27], distinguishable from the scattered light.

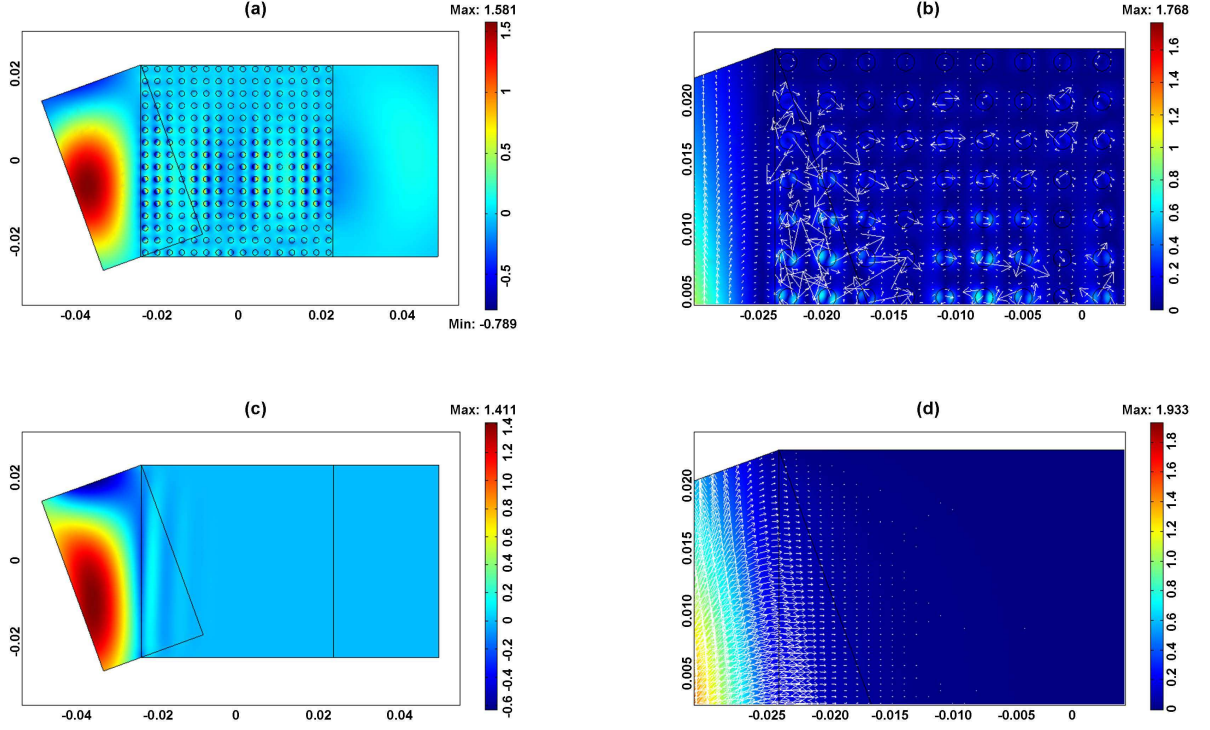


FIG. 3. (a) Electric field $E_z(\mathbf{R})$ spatial distribution of a microwave propagating through a slab of an ordered array of BST rods as the one of Figs. 1(a) - (c) ($\epsilon = 600$, $r = 0.68mm$). The lattice constant is $a = 3mm$. An s - polarized Gaussian beam of amplitude $A = 1V/m$ and width $\sigma = 4a$ is launched on the PC from the left at wavelength $\lambda = 41.638mm$ ($\nu = 7.2GHz$) and at an incidence angle $\theta = 20^\circ$ with the X - axis. (b) Electric field norm $|E_z(\mathbf{R})|$ (colors) and $\langle \mathbf{S}(\mathbf{R}) \rangle$ (arrows) in a detail of the block upper left corner. (c) Same as in (a) in a slab occupied by a homogeneous medium whose effective parameters obtained from the EMT are $\epsilon_{eff} = -36 + i14.7$, $\mu_{eff} = -0.9 + i0.11$. (d) Electric field norm $|E_z(\mathbf{R})|$ (colors) and $\langle \mathbf{S}(\mathbf{R}) \rangle$ (arrows) in a detail of the block upper left corner.

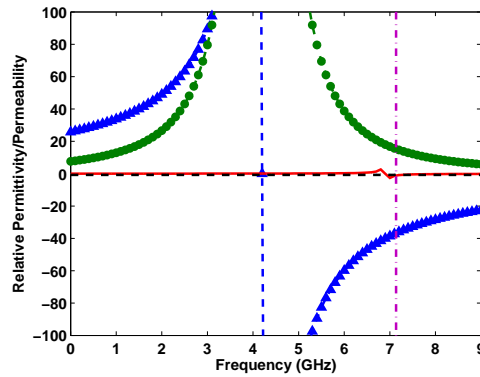


FIG. 4. Estimation of both the complex relative permittivity ϵ_{eff} and permeability μ_{eff} for the BST rod array in Fig. 3(a) obtained the effective medium theory. ϵ_{eff}^R (broken line with triangles. Blue online), ϵ_{eff}^I (broken line with dots. Green online), μ_{eff}^R (full line. Red online) and μ_{eff}^I (broken line. Black online). The broken with dots vertical line (violet online) at frequency $\nu = 7.2GHz$ indicates both ϵ_{eff} and μ_{eff} values for the medium of Figs. 3(c) and 3(d): $\epsilon_{eff} = -36$, $\epsilon_{eff}^I = 14.7$, $\mu_{eff}^R = -0.9$ and $\mu_{eff}^I = 0.11$. The full vertical (blue online) line belongs to the jump of ϵ_{eff}^R .

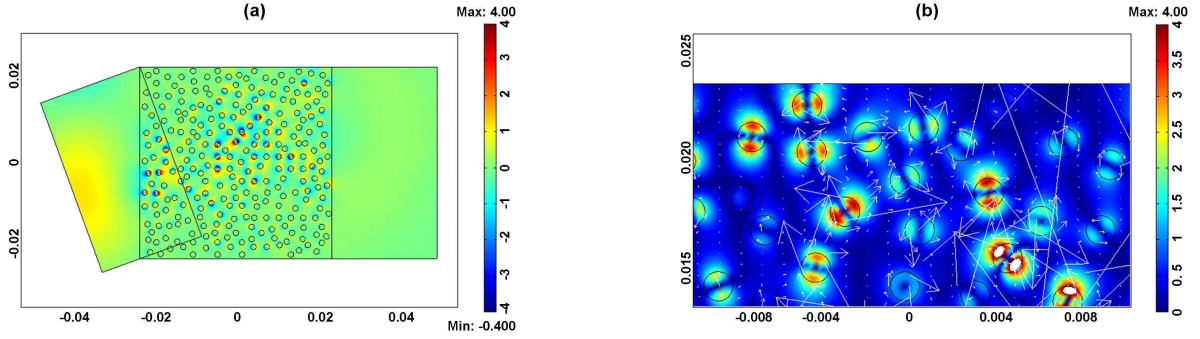


FIG. 5. (a) Electric field $E_z(\mathbf{R})$ spatial distribution in a random configuration of cylinders like those of Figs. 1(a) - (c) keeping the same filling fraction and the same conditions of illumination as in the ordered array of Figs. 3. (b) Electric field norm $|E_z(\mathbf{R})|$ (colors) and $\langle \mathbf{S}(\mathbf{R}) \rangle$ (arrows) in a detail of the block central region which includes its upper transparent side.

Ordered and random distributions of Silicon rods in the mid - infrared regime

We next address a thick slab of ordered Si cylinders like that studied in Figs. 2. This arrangement is an extension to mid - IR ([12]) of the previous calculations at microwaves discussed in Sections ?? and ?. As shown in Figs. 6(a) and 6(b) there appears negative refraction (i. e. a backward wave) in the block and no appreciable transmission losses. The positive and negative peak values of the wavefronts transmitted inside the array coincide with those cylinders that appear resonantly illuminated thus exhibiting the Mie $T_{1,1}$ resonance like in Fig. 2(a). Mainly, there are $\langle \mathbf{S}(\mathbf{R}) \rangle$ arrows pointing in the direction normal to these wavefronts. Light is transmitted into the air side on the right through this slab with the same angle as that of incidence. This confirms the analysis of [12] for this crystal.

On the other hand, Figs. 6(c) and 6(d) display the transmission of the same incident wave through a thick slab occupied by a uniform medium with a refractive index: $n = -0.36 + i0.25/8$ which resembles the propagation through the ordered array shown in Figs. 6(a) and 6(b). The real part $n^R = -0.36$ has been estimated from Snell's law applied to Fig. 6(a), whereas the imaginary part $n^I = 0.25/8$ was fitted to a transmittance of this homogeneous medium being approximated to that of Figs. 6(a) and 6(b). Notice that the transmittivity of the homogeneous slab of Figs. 6(c) and 6(d) is smaller than that of the ordered array of Figs. 6(a) and 6(b). However n^I cannot decrease much beyond $0.25/8$, since otherwise well known instabilities due to divergences at the right side of the slab [28–30] appear. However, it should be remarked that this value of n does not coincide with that of an EMT, which according to the values of a/λ and r/λ for this array, as discussed in Section ??, are too large for a homogenization procedure to work with such a structure. This is further discussed next by employing other arrays of these cylinders with the same filling fraction and lattice parameter; namely, a thick slab of disordered Si rods and a prism of ordered, or disordered, cylinders.

When these cylinders are disordered keeping $f \approx 0.30$, as seen in Figs. 7(a) - (c), there is no such negative refraction inside the block as that shown in Figs. 6. Now there is a huge extinction of energy due to high scattering by the particles. By averaging over several realizations, there is no observed refractive transmission of a forward component $\langle \mathbf{E}_z \rangle$ into the air side. The block of disordered rods now scatters, see Figs. 7(a) and 7(b), more than 90% of the transmitted intensity both above and below its upper and lower low reflection boundaries. Hence, only some few spheres are illuminated showing their $TM_{1,1}$ Mie resonances. Figure 7(c) shows that $|\langle \mathbf{S}(\mathbf{R}) \rangle|$ is transmitted into the air region at the right of the slab with less than a 1/10 of its incident wave value.

A prism of ordered or disordered Si distributions in the infrared

Let us consider now a prism of a uniform medium of refractive index $n = -0.36 + i0.25/8$. Notice that this value of n is the one of Figs. 6(c) and 6(d), derived from refraction at the ordered array of Figs. 6(a) and 6(b). As shown in Figs. 8, refraction into the air takes place with $\theta_i = 18.4^\circ$ and $\theta_t = 38.07^\circ$, the latter being the negative angle of refraction at the prism larger side. This is shown in Figs. 8(a) - (c) and serves us as a reference to study transmission through both an ordered and disordered array of Si rods contained in a sample with this prism geometry, which also was the one employed in transmission observations at microwaves in [11].

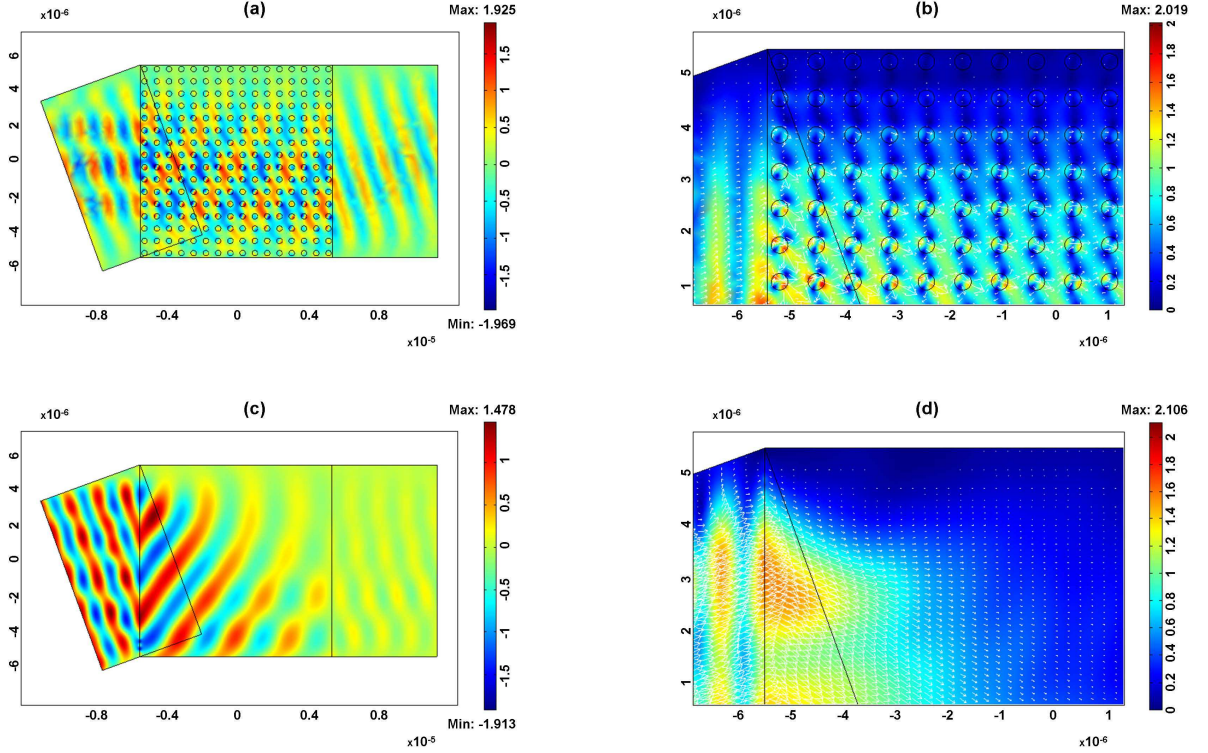


FIG. 6. (a) Electric field $E_z(\mathbf{R})$ propagating in a thick slab occupied by an ordered array of Si rods ($\epsilon = 12$ and $r = 158nm$; the lattice constant is $a = 698nm$). An s - polarized Gaussian beam of amplitude $A = 1V/m$, $\sigma = 4a$ and wavelength $\lambda = 1.55\mu m$ is launched on the slab from the left at an incidence angle $\theta = 20^\circ$. (b) Electric field norm $|E_z(\mathbf{R})|$ (colors) and $\langle \mathbf{S}(\mathbf{R}) \rangle$ (arrows) in a detail of the block upper left corner. (c) Electric field $E_z(\mathbf{R})$ in a uniform medium optically equivalent to that of (a) and (b), whose electric permittivity is $\epsilon_{eff} = -0.36 + i0.25/8$. The real part of such a value is estimated by Snell's law, ($\theta_i = 21.54^\circ$, $\theta_t = 38.07^\circ$). The imaginary part has been estimated from the transmittivity of Figs. 6(a) and 6(b). (d) Electric field norm $|E_z(\mathbf{R})|$ (colors) and $\langle \mathbf{S}(\mathbf{R}) \rangle$ (arrows) in a detail of the block upper left corner.

Figures 9(a) - (c) show the wave propagation on illumination of the prism filled with an ordered array of Si cylinders identical to that of the thick slab of Figs. 6(a) and 6(b). As shown, there is now absence of negative refraction at the larger side interface of this prism. This contrasts with the observation in the sample with the same shape filled with a uniform medium, as displayed in Figs. 8(a) - (c) and also with the case of a thick slab filled with the same array, as seen in Figs. 6(a) and 6(b). Hence, at difference with the crystal of Si rods in the block, the same crystal in the prism does not reproduce negative refraction, but rather a set of diffracted orders into the air which are associated to the prism angle α , according to the conservation of the transversal wavevectors at the larger interface. Also, the wave propagation inside the prism, which should be like that appearing in the thick slab of Fig. 6(a), but now at the same direction as the incident wave, (since now this latter wave incides on the prism at $\theta_i = 0^\circ$), is observed in Figs. 9(a) and 9(b) to be quite different, with a complicated structure due to the interference of the different Bragg waves. This result, once again, points out the dependence of wave propagation not only on the inner structure of the composite, but also on its shape. In addition, these observations demonstrate that the negative refraction found in the slab of ordered Si rods, (cf. Fig. 6(a)) is not due to an effective homogeneous medium effect, but it rather comes from a consequence of the diffraction in the array of Si rods due to its lattice symmetry. This answers the question posed in [18].

This latter remark is further confirmed by disordering this Si cylinder array within the prism, (see Figs. 10(a) - (c)). Again, no refracted beam into the air is observed, and a large portion of energy is lost by scattering from the composite elements. Many outgoing beams mix with each other, so that no forwardly transmitted beam inside the prism, characterized by $\langle E_z(\mathbf{R}) \rangle$ can be distinguished by averaging over several realizations of the random array. The apparent refracted beam at $\theta_t = 0^\circ$ shown in the air side exiting the prism, changes as one varies the random realization of rods.

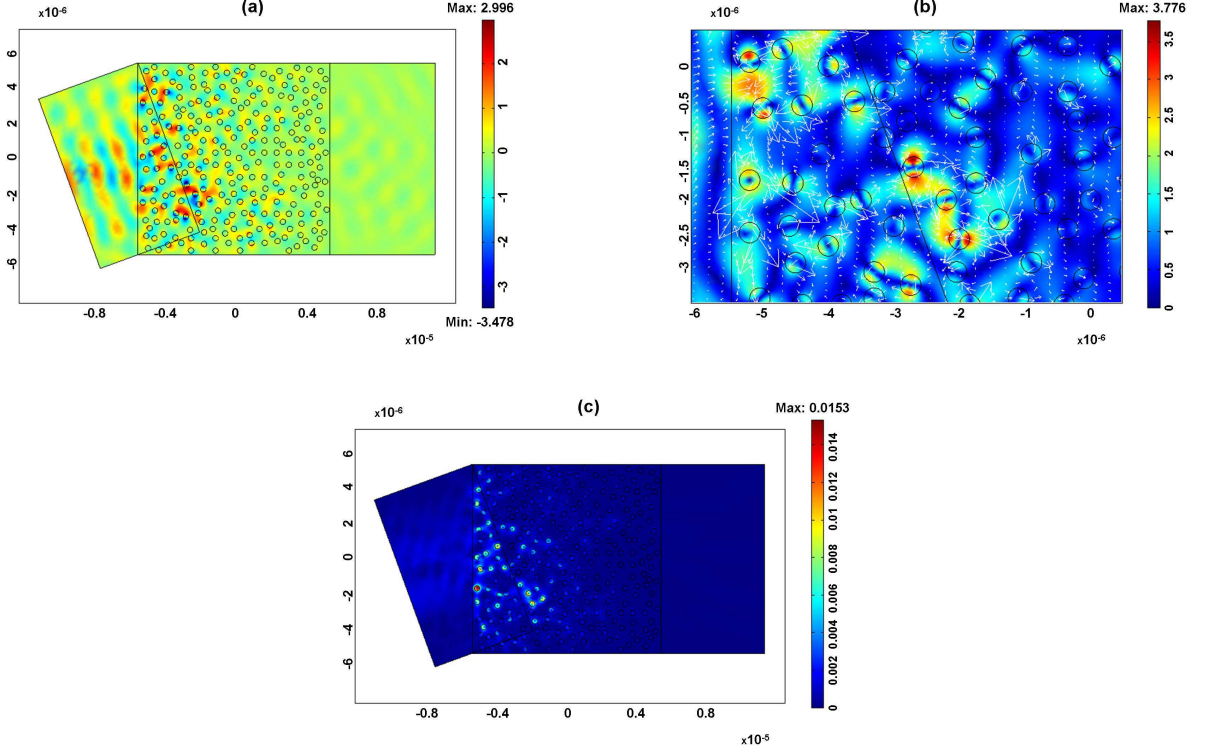


FIG. 7. (a) Electric field $E_z(\mathbf{R})$ when the configuration of Si rods shown in Figs. 6(a) and 6(b) is disordered, keeping the same filling fraction $f = 0.30$ and the same conditions of illumination. (b) Electric field norm $|E_z(\mathbf{R})|$ (colors) and $\langle \mathbf{S}(\mathbf{R}) \rangle$ (arrows) in an inset of the block left region which includes its left interface. (c) Map of the averaged energy flow norm $|\langle \mathbf{S}(\mathbf{R}) \rangle|$.

CONCLUSIONS

In this paper we have assessed the transmittance of composites of dielectric particles whose Mie resonance electric and magnetic modes were proposed by previous extensive studies to yield negative refraction. We have shown that such structures cannot be homogenized neither reproduce the propagation observed in the frequency regions of study. In this way, we have proved that the negative refraction previously found in ordered arrays is thus a diffraction effect which disappears as soon as the particle distribution is randomized, and does not reproduce the transmission of their corresponding EMT uniform media, this was an open question so far.

In addition, we conclude, first, that the effective parameters obtained from a homogenization theory, do not reproduce the propagation observed through an ordered array of these elements. This is further seen when these arrays are randomized. If an EMT worked, it should not depend on whether the “meta - atom” distributions were ordered or disordered. Then strong scattering by disordered rods extinguishes most of the incident energy, and there is not negatively refracted forward beam observed.

Second, the behavior of the transmitted beam in ordered arrays also depends on the shape of the sample and hence does not match with an EMT which does not include this shape. These conclusions are consistent with the well known *difficulty of working out EMTs within the frequency range of resonance of the composite elements* [16]. Similar consequences should hold for 3D composites of resonant dielectric spheres.

ACKNOWLEDGEMENTS

We thank J. J. Sáenz and L. Froufe for stimulating and useful discussions on this subject. Research supported by the Spanish MiCINN through FIS2009-13430-C02-C01 and Consolider NanoLight (CSD2007-00046) research contracts. The latter grant supports the work of FJVV.

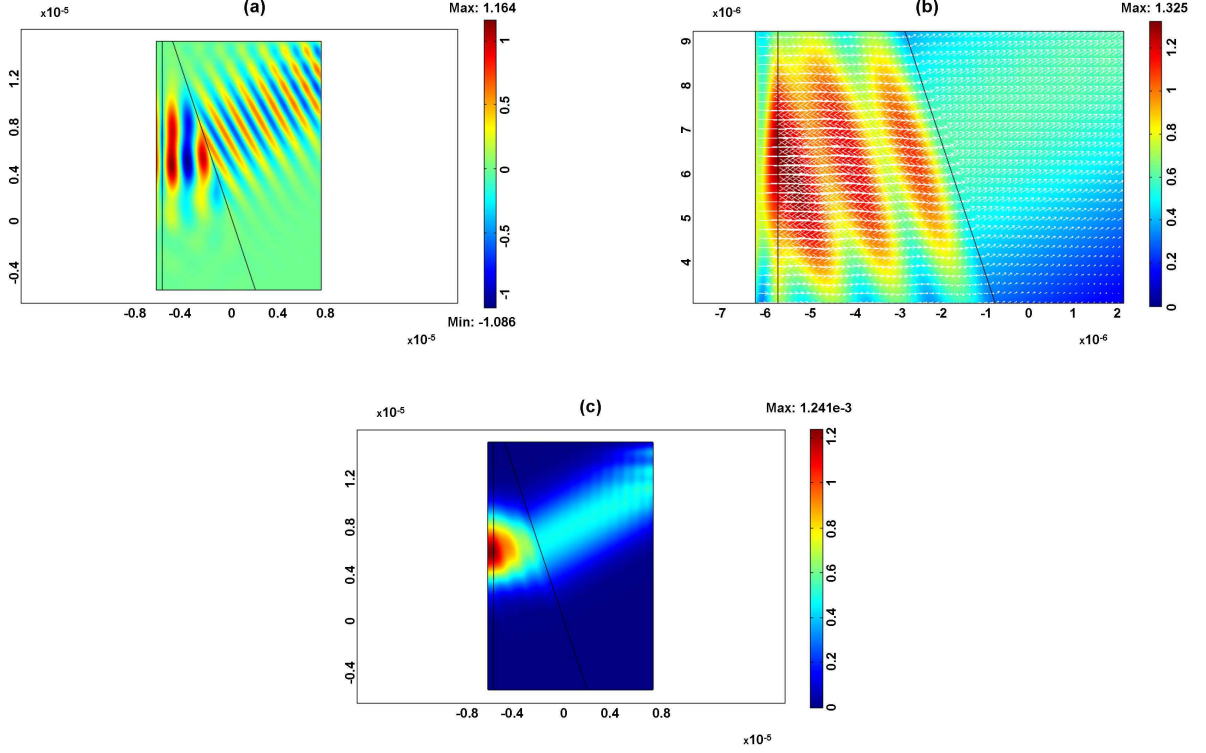


FIG. 8. (a) Electric field $E_z(\mathbf{R})$ in a prism (top angle $\alpha = 18.4^\circ$) occupied by a uniform medium whose electric permittivity is $\epsilon_{eff} = -0.36 + i0.25/8$ illuminated from the left. This prism is optically as dense as the homogeneous thick slab of Figs. 6(c) and 6(d). (b) Electric field norm $|E_z(\mathbf{R})|$ (colors) and $\langle \mathbf{S}(\mathbf{R}) \rangle$ (arrows) in a detail of the prism upper region. (c) Map of the averaged energy flow norm $|\langle \mathbf{S}(\mathbf{R}) \rangle|$. An s - polarized Gaussian beam of amplitude $A = 1V/m$, $\sigma = 4 \times 698nm$ and wavelength $\lambda = 1.55\mu m$ is launched from the left on the prism at $\theta_i = 0^\circ$ with its left side.

-
- [1] D. R. Smith, S. Schultz, P. Markos and C. M. Soukoulis, Determination of effective permittivity and permeability of metamaterials from reflection and transmission coefficients, Phys. Rev. B 65 (2002) 195104.
 - [2] A. Alu and N. Engheta, Achieving transparency with plasmonic and metamaterial coatings, Phys. Rev. E 72 (2005) 016623.
 - [3] D. R. Smith et al., Electromagnetic parameter retrieval from inhomogeneous metamaterials, Phys. Rev. E 71 (2005) 036617.
 - [4] C. M. Soukoulis, M. Kafesaki and E. N. Economou, Negative-index materials: new frontiers in optics, Adv. Mater. 18 (2006) 1941.
 - [5] C. M. Soukoulis, S. Linden and M. Wegener, Negative refractive index at optical wavelengths, Science 315 (2007) 47.
 - [6] J. Zhou, T. Koschny and C. Soukoulis, An efficient way to reduce losses of left-handed metamaterials, Opt. Express 16 (2008) 11147.
 - [7] J. Valentine, J. Li, T. Zentgraf, G. Bartal and X. Zhang, An optical cloak made of dielectrics, Nat. Materials (2009) 2461.
 - [8] M. S. Wheeler, J. S. Aitchison and M. Mojahedi, Three-dimensional array of dielectric spheres with an isotropic negative permeability at infrared frequencies, Phys. Rev. B 72 (2005) 193103.
 - [9] M. S. Wheeler, J. S. Aitchison and M. Mojahedi, Coated nonmagnetic spheres with a negative index of refraction at infrared frequencies, Phys. Rev. B 73 (2006) 045105.
 - [10] J. A. Schuller, R. Zia, T. Taubner and M. Brongersma, Dielectric metamaterials based on electric and magnetic resonances of silicon carbide particles, Phys. Rev. Lett. 99 (2007) 107401.
 - [11] L. Peng, L. Ran, H. Chen, H. Zhang, J. A. Kong and T. Grzegorzcyk, Experimental observation of left-handed behavior in an array of standard dielectric resonators, Phys. Rev. Lett. 98 (2007) 157403.
 - [12] K. Vynck, D. Felbacq, E. Centeno, A. I. Cabuz, D. Cassagne and B. Guizal, All-dielectric rod-type metamaterials at optical frequencies, Phys. Rev. Lett. 102 (2009) 133901.
 - [13] A. García - Etxarri, R. Gómez - Medina, L. S. Froufe - Pérez, C. López, L. Chantada, F. Scheffold, J. Aizpurua, M. Nieto - Vesperinas and J. J. Sáenz, Strong magnetic response of submicron silicon particles in the infrared, Opt. Express 19 (2011) 4815.

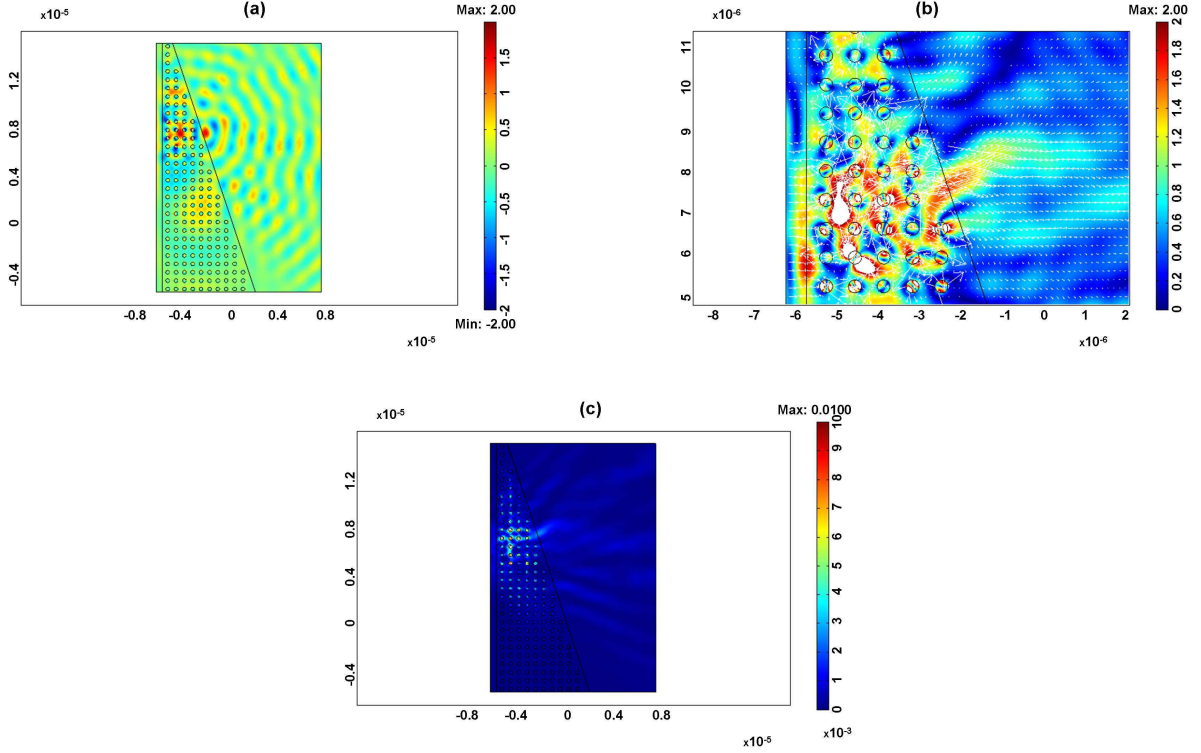


FIG. 9. (a) Electric field $E_z(\mathbf{R})$ in a prism with the same shape as that of Figs. 8(a) - (c), at the same illumination conditions, but now occupied by an ordered Si rod array as that of Figs. 6(a) and 6(b). (b) Electric field norm $|E_z(\mathbf{R})|$ (colors) and $\langle \mathbf{S}(\mathbf{R}) \rangle$ (arrows) in a detail of the prism upper region. (c) Averaged energy flow norm $|\langle \mathbf{S}(\mathbf{R}) \rangle|$. The illumination is the same as in Figs. 8(a) - 8(c).

- [14] M. Notomi, Theory of light propagation in strongly modulated photonic crystals: refractionlike behavior in the vicinity of the photonic band gap, *Phys. Rev. B* 62 (2000) 10696.
- [15] X. H. Zhang and S. R. Forrest, Generalized phase matching condition for lossy periodic photonic structures, *Opt. Express* 18 (2010) 1151.
- [16] X. H. Zhang and S. R. Forrest, Theory of the perfect lens, *Phys. Rev. B* 84 (2011) 045427.
- [17] X. H. Zhang, M. Davanco, Y. Urzhumov, G. Schvets and S. Forrest, From scattering parameters to Snells law: a subwavelength near-infrared negative-index metamaterial, *Phys. Rev. Lett.* 101 (2008) 267401.
- [18] Q. Zhao, J. Zhou, F. Zhang and D. Lippens, Mie resonance-based dielectric metamaterials, *Materials Today* 12 (2009) 60.
- [19] N. Fabre, L. Lalouat, X. Melique, F. de Fornel and O. Vanbesien, Optical near-field microscopy of light focusing through a photonic crystal flat lens, *Phys. Rev. Lett.* 101 (2008) 073901.
- [20] R. A. Shelby, D. R. Smith and S. Schultz, Experimental verification of a negative index of refraction, *Science* 292 (2001) 77.
- [21] M. Sanz, A. Papageorgopoulos, W. E. Egelhoff, M. Nieto - Vesperinas and N. García, Transmission measurements in wedge-shaped absorbing samples: an experiment for observing negative refraction, *Phys. Rev. E* 67 (2003) 067601.
- [22] L. Lewin, The electrical constants of a material loaded with spherical particles, *Proc. IEE* 94 (1948) 65.
- [23] C. L. Holloway, E. F. Knester, J. B. Jarvis and P. Kabos, A double negative (DNG) composite medium composed of magnetodielectric spherical particles embedded in a matrix, *IEEE Trans. Antennas Propag.* 51 (2003) 2596.
- [24] A. Ishimaru, Wave propagation and scattering in random media vols 1 and 2, first ed., Academic Press, New York, 1997.
- [25] A. Garcia-Martin, J. A. Torres, J. J. Saenz y M. Nieto-Vesperinas, Transition from diffusive to localized regimes in surface corrugated optical waveguides, *Appl. Phys. Lett.* 71 (1997) 1912-1914.
- [26] J. Riley, H. Dehghani, M. Schweiger, S. R. Arridge, J. Ripoll y M. Nieto-Vesperinas, 3D optical tomography in the presence of void regions, *Opt. Express* 7 (2000) 462-467.
- [27] J. Ripoll, M. Nieto-Vesperinas, V. Ntziachristos, J. P. Culver, D. N. Pattanayak y A. G. Yodh, Recovery of optical parameters in multiple layered diffusive media: theory and experiments, *J. Opt. Soc. Am. A* 18 (2001) 821-830.
- [28] R. W. Ziolkowski and E. Heyman, Wave propagation in media having negative permittivity and permeability, *Phys. Rev. E* 64 (2001) 056625.
- [29] N. García and M. Nieto - Vesperinas, Left-handed materials do not make a perfect lens, *Phys. Rev. Lett.* 90 (2002) 229903.

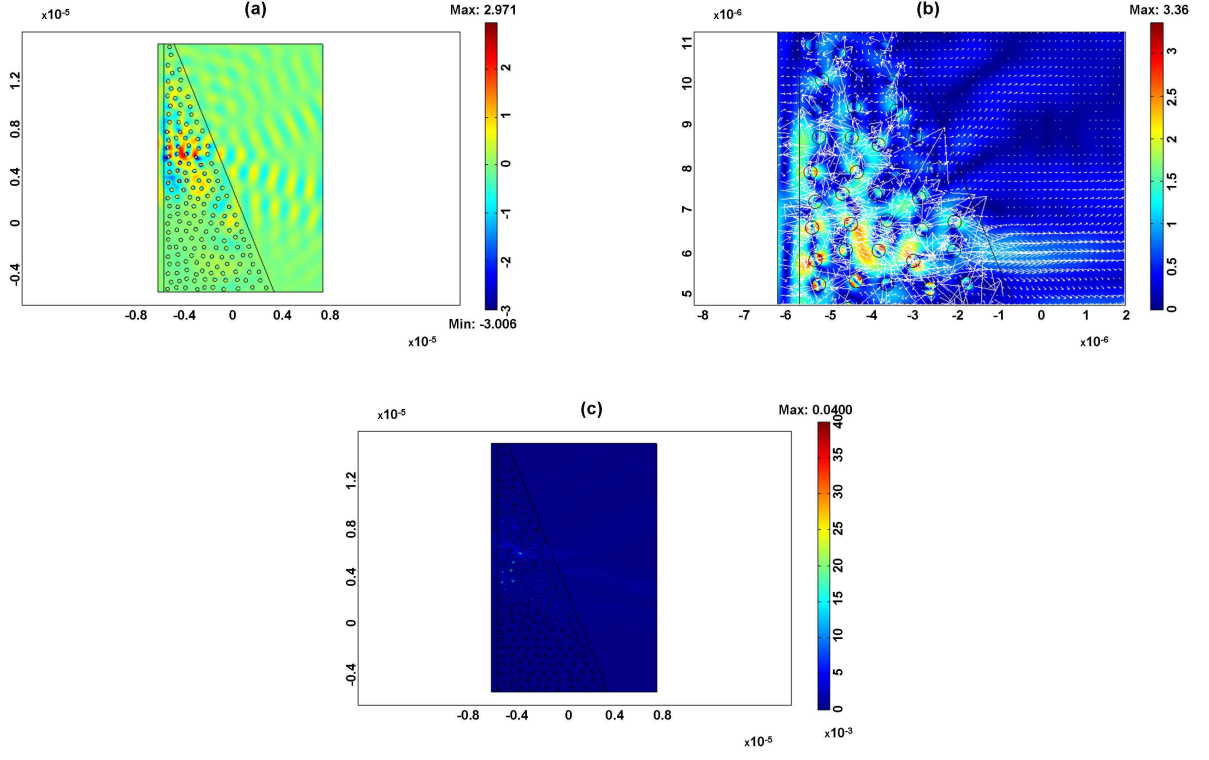


FIG. 10. (a) Electric field $E_z(\mathbf{R})$ in the configuration shown in Figs. 9(a) - (c), (now with a top angle $\alpha = 22^\circ$), the Si rod array being now randomized but keeping the same filling fraction $f = 0.30$ as in the ordered array. The conditions of illumination are the same as in Figs. 8(a) - 8(c). (b) Electric field norm $|E_z(\mathbf{R})|$ (colors) and $\langle \mathbf{S}(\mathbf{R}) \rangle$ (arrows) in a detail of the prism upper area. (c) Averaged energy flow norm $|\langle \mathbf{S}(\mathbf{R}) \rangle|$.

- [30] M. Nieto - Vesperinas, Problem of image superresolution with a negative-refractive-index slab, J. Opt. Soc. Am. A 21 (2004) 491.